Large enhancement and uniform distribution of optical near field through combining periodic bowtie nanoantenna with rectangular nanoaperture array

Jianxiong Li,[1] Shuqi Chen,[1,*] Ping Yu,[1] Hua Cheng,[1] Wenyuan Zhou,[1] and Jianguo Tian[1,2]

[1]*The Key Laboratory of Weak Light Nonlinear Photonics, Ministry of Education, School of Physics and Teda Applied Physics School, Nankai University, Tianjin 300457, China*

[2]*e-mail: jjtian@nankai.edu.cn*

**Corresponding author: schen@nankai.edu.cn*

Received July 8, 2011; revised September 13, 2011; accepted September 15, 2011; posted September 19, 2011 (Doc. ID 150687); published October 6, 2011

We present a novel (to the best of our knowledge) composite nanostructure composed of bowtie nanoantennas (BNAs) and rectangular nanoapertures, which provides a new way to improve the ability of the nanostructure to enhance the optical near field and obtain uniform near-field distribution in the z direction. It is specifically engineered to not only confine the incident light in the nanoscale but also to generate large localized near-field enhancement about 25 times larger than that of solitary BNAs. It also shows a more uniform near-field distribution in the z direction than that of solitary BNAs. The mechanisms of the large enhancement and the uniform near field are also discussed.

OCIS codes: 160.3918, 240.6680, 310.6628.

The development of metamaterials has led to the realization of phenomena that cannot be obtained with natural materials. The ability of some metamaterials to confine light to the nanometer scale with high intensity is of great interest to studies of light interactions with biological materials [1] and nanostructures [2] as well as some potential applications such as nanolithography [3], fluorescence enhancement [4], and surface-enhanced Raman scattering [5,6]. There are two kinds of nanostructures: nanoantennas [7,8] and nanoapertures [9], which can concentrate and enhance the optical near field. As we know, the optical near field of bowtie nanoantennas (BNAs) can be enhanced tremendously by the plasmonic resonance and curvature effect of bowtie tips. BNAs have been shown to exhibit higher localized field enhancement and better spatial confinement of the applied electric field than other coupled-plasmon resonant-nanoparticle pair geometries [10]. On the other hand, bowtie nanoapertures have also been proposed as an alternative solution to BNAs for efficiently concentrating light down to the nanoscale level [9,11,12] or generating extraordinary transmission [13]. Because of the limitation of the enhancement mechanism, there is seldom an alternative way to improve the level of enhancing the optical near field, besides to design the metamaterial structure with the smaller gap [14] or sharper angle [15]. However, both of these nanostructures have reached current fabrication limits or need a very complicated fabrication process.

In this Letter, we propose a composite nanostructure composed of periodic BNAs and rectangular nanoapertures (RNAs), termed a combination of BNAs and RNAs (CBRs), which provides a new way of improving the ability of the nanostructure to enhance the optical near field without inducing too much complexity. It is demonstrated that CBRs exhibit three resonant peaks due to the interaction between BNAs and RNAs, which can generate a larger localized near-field enhancement than that of solitary BNAs. Meanwhile, the incident light can be highly confined in nanoscale with a uniform near-field distribution along the z axis. When the BNA is located near the middle region of the nanoaperture, the localized intensity can be simultaneously enhanced around three resonant peaks to form a broadband enhancement. Moreover, the incident light can be well confined in the gap of the BNA at arbitrary position of normalized intensity spectrum, which is more uniform and symmetric than previous research results. The mechanism of the large enhancement and the uniform near field are also discussed.

A schematic illustration of CBRs is shown in Fig. 1. The Au layer with RNA is placed on the glass layer in the unit cell. A 20 nm thick BNA is located at the bottom of the RNA. Two symmetry axes of the BNA are overlapped with those of RNA. Each constituent Au equilateral triangle of the bowtie has a perpendicular bisector length of 40 nm with a 6.3 nm curvature radius at corner. The permittivity of gold is described by the Drude model with the relative permittivity at infinite frequency $\varepsilon_\infty = 9.0$, the plasma frequency $\omega_p = 1.3166 \times 10^{16}\,\mathrm{s}^{-1}$, and the damping constant $\gamma = 1.3464 \times 10^{14}\,\mathrm{s}^{-1}$ [16]. The permittivity of the glass substrate is taken as 2.25. The electromagnetic resonance and local intensity enhancement of CBRs are studied by the finite element method using COMSOL Multiphysics [17]. The plane wave is incident from the top (air side) and normal to the CBR surface with electric field component amplitudes of $e_x = 1$,

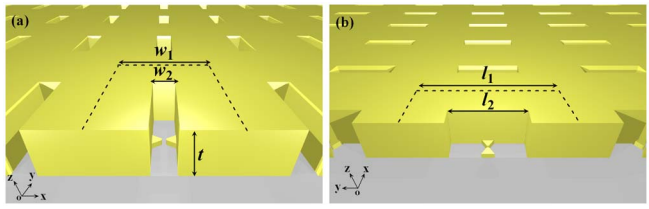

Fig. 1. (Color online) Schematic illustration of CBRs from cross sections: (a) x–y plane, $w_1 = 400$ nm, $w_2 = 80$ nm, $t = 160$ nm and (b) y–z plane, $l_1 = 650$ nm, $l_2 = 292$ nm.

$e_y = 0$, $e_z = 0$, which is parallel to the pair of triangles. Perfectly matched layers are used at the top and bottom of the simulation domain to completely absorb waves, leaving the simulation domain in the direction of propagation. Periodic boundary conditions are used in the x and y directions. The near-field intensity spectra are plotted by the maximum normalized e-field intensity within the plane through the center of the BNA in the z direction at each wavelength.

A number of recent publications have discussed the extraordinary transmission properties of nanoapertures, but the characteristic of local field enhancement is ignored because of their undesirable effect, for instance, the local intensity of RNAs in our design can just enhance about 90 times at 630 nm [as shown in Fig. 2(a)]. In addition, the normalized intensity spectrum of RNAs shows two distinct resonant peaks, which can lead CBRs to have more than one resonant peak [as shown in Fig. 2(b)]. On the other hand, BNAs have a strong resonant peak at 640 nm, and its local intensity enhancement can reach about 750 times, following the previous result in [18]. To reveal the differences of the enhanced local intensity between BNAs/RNAs and CBRs, we calculated the normalized near-field intensity spectra for BNAs, RNAs, and CBRs in Fig. 2(b). It reveals that the normalized intensity spectra of CBRs have three peaks. The resonant peak P_3 of CBRs is the strongest among the three resonant peaks, and the local intensity enhancement at P_3 is about 25 times larger than that of BNAs. Meanwhile, the resonant peak P_3 of CBRs has a redshift compared with that of BNAs due to the coupling between the BNA and RNA. Furthermore, the near-field distribution of BNAs in the gap region at the resonant peak is located near the glass/metal interface along the z axis because of the different dielectric constants on both sides of the BNAs and normal illumination, which is shown in the insets of Fig. 2(a). This nonuniform distribution was also reported in the diabolo nanoantenna structure [19]. However, CBRs show a more uniform near-field distribution in the gap region along the z axis at resonant peak P_3 [as shown in the insets of Fig. 2(b)]. This discrepancy is attributed to the difference of the incident angle. The solitary BNAs are illuminated by normal incident light. However, the BNAs in CBRs are illuminated by incident light with different incident angles due to the multiply reflection of the incident light in CBRs. Therefore, a more uniform field distribution along z axis is obtained in CBRs. The impact of resonant cavities in optical phenomenon also has been explored in [20,21].

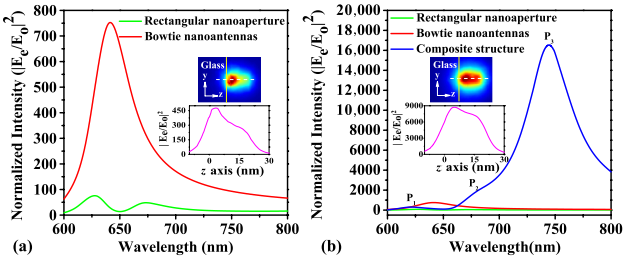

Fig. 2. (Color online) (a) Calculated normalized intensity spectra for BNAs and RNAs. (b) Comparison of normalized intensity spectra between the BNAs/RNAs and CBR. Insets, normalized near-field distribution of (a) BNAs and (b) CBRs in the gap region along the z axis and cut line plot along the dashed line, which does not correspond to the maximal normalized intensity.

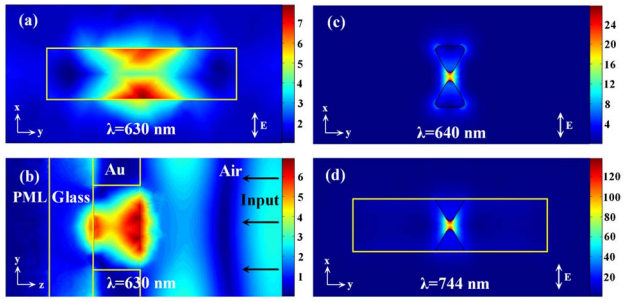

Fig. 3. (Color online) Calculated normalized near-field distribution at the resonant peak wavelength for (a) RNAs—the cutting plane is 10 nm away from the bottom of the RNAs, (b) RNAs —the cutting plane is in the middle of the RNAs in x–y plane, (c) BNAs in the transverse x–y plane, and (d) CBR in the transverse x–y plane.

To further understand the differences of near-field distribution, we give the normalized near-field spatial distribution for BNA, RNA, and CBR at the main resonant wavelength in Fig. 3. Results show that the RNA not only can generate a wide near-field distribution [see in Fig. 3(a)], but it also can confine the incident light into the nanoaperture [see in Fig. 3(b)] due to the guided mode inside the nanoaperture [22]. BNA can make a strong enhancement and concentrate the light in nanoscale in its gap region [see in Fig. 3(c)] when the incident radiation polarization is parallel to the pair of triangles. It is these capacities of both RNAs and BNAs that make the CBRs realize a larger enhancement than that of solitary BNAs. The large near-field enhancement can be explained by the double interaction between the composite structure and incident light. First, the incident light is coupled into RNAs by adjusting a reasonable aperture size. Then, the concentrated near fields in RNAs have been further enhanced by BNAs, which result in a large near-field enhancement for CBRs. However, it should be emphasized that this kind of large enhancement arises from some complex coupling effects in CBRs, not only a simple superposition between RNAs and BNAs. The normalized near-field distribution for CBRs at resonant wavelength 744 nm is given in Fig. 3(d). As expected, most of the e-fields for CBRs are assembled near the gap region of the BNA and still retain a nanoscale mode volume, which are consistent with those of solitary BNAs.

Numerical results about CBRs show a large localized intensity enhancement and a capability that can symmetrically concentrate light to the nanoscale along the z axis near the gap of BNAs in CBRs. In order to explore the origin of three resonant peaks and obtain more symmetrical concentrated light, we lift BNAs in CBRs a distance along the z axis, which is defined as d in the inset of Fig. 4(a). Figure 4(a) shows the normalized near-field spectra for the different distance d. Meanwhile, we also give the position of three resonant peaks for the different distance d in Fig. 4(a). Results show that the position and the relative amplitude of the resonant peaks can be obviously affected by the distance d of the BNA. As the distance d increases from 50 to 140 nm, the resonant peak

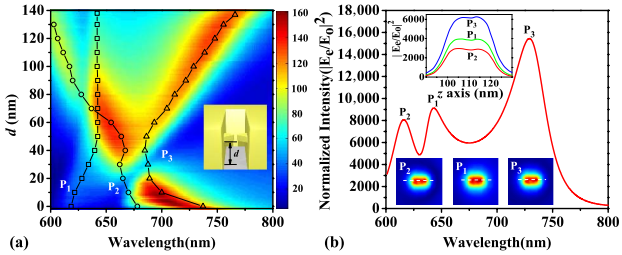

Fig. 4. (Color online) (a) The normalized near-field spectra and position of three resonant peaks of CBRs as a function of d. (b) The normalized intensity spectra of the CBRs when d is 100 nm. Insets, (a) the definition of distance d and (b) the normalized near-field distribution of CBRs in the gap region along the z axis and cut line plot along the dashed line, where it does not correspond to the maximal normalized intensity.

P_1 is fixed at 640 nm, which is equal to the resonance wavelength of solitary BNAs. However, the resonant peaks P_2 and P_3 shift apparently as the transverse distance d increases. When the BNA is lifted closer to the top of the RNA, the external e-field of the BNA in CBR is very similar to that of the solitary BNA. Therefore, the resonant peak P_1 is the intrinsic resonance of BNAs in CBRs. On the other hand, two peaks P_2 and P_3 of CBRs arise from two guided modes of RNAs. When the BNA is located near the middle region of the nanoaperture, the localized intensity can be simultaneously enhanced around three resonant peaks to form a broadband enhancement, as shown in Fig. 4(b). The insets of Fig. 4(b) show the near-field distribution and corresponding cut line plot for several featured positions. The incident light can be well confined in the gap of the BNA along the z axis at an arbitrary position of the normalized intensity spectrum, which is more uniform and symmetric than that in the insets of Fig. 2(b).

In conclusion, we designed novel (to the best of our knowledge) composite nanostructure CBRs composed of BNAs and RNAs. The proposed CBRs not only can create a highly localized large near field in optical frequencies, but it also can have a more uniform near-field distribution than that of solitary BNAs in the gap region along the z axis. CBRs exhibit three distinct resonance frequencies due to the complex coupling effects between BNAs and RNAs. We demonstrated that one of them is contributed by the intrinsic resonance of BNAs in CBRs and the others are from the guided modes of RNAs. Structures of this type can be readily fabricated either by a focused ion beam or electron beam lithography, similar to the fabrication of BNAs and RNAs. Based on its capabilities, CBRs are expected to have a profound impact on a wide range of optoelectronic and plasmonic applications, including ultrafast color-sensitive photodetection, solar power light harvesting, super-resolution imaging, and enhanced Raman spectroscopy.

This work is supported by the Chinese National Key Basic Research Special Fund (grant 2011CB922003), the Natural Science Foundation of China (NSFC) (grants 10974103 and 61008002), the Specialized Research Fund for the Doctoral Program of Higher Education (grant 20100031120005), the Fundamental Research Funds for the Central Universities (grant 65010801), and the 111 Project (grant B07013).

References

1. E. J. Sanchez, L. Novotny, and X. S. Xie, Phys. Rev. Lett. **82**, 4014 (1999).
2. P. Biagioni, J. S. Huang, L. Duò, M. Finazzi, and B. Hecht, Phys. Rev. Lett. **102**, 256801 (2009).
3. Y. Zhang, X. Dong, J. Du, X. Wei, L. Shi, Q. Deng, and C. Du, Opt. Lett. **35**, 2143 (2010).
4. A. Kinkhabwala, Z. F. Yu, S. H. Fan, Y. Avlasevich, K. Mullen, and W. E. Moerner, Nat. Photon. **3**, 654 (2009).
5. M. G. Banaee and K. B. Crozier, Opt. Lett. **35**, 760 (2010).
6. P. Dawson, J. A. Duenas, M. G. Boyle, M. D. Doherty, S. E. J. Bell, A. M. Kern, O. J. F. Martin, A. S. Teh, K. B. K. Teo, and W. I. Milne, Nano Lett. **11**, 365 (2011).
7. A. Sundaramurthy, K. B. Crozier, G. S. Kino, D. P. Fromm, P. J. Schuck, and W. E. Moerner, Phys. Rev. B **72**, 165409 (2005).
8. K.-P. Chen, V. P. Drachev, J. D. Borneman, A. V. Kildishev, and V. M. Shalaev, Nano Lett. **10**, 916 (2010).
9. E. X. Jin and X. F. Xu, Appl. Phys. Lett. **88**, 153110 (2006).
10. D. P. Fromm, A. Sundaramurthy, P. J. Schuck, G. Kino, and W. E. Moerner, Nano Lett. **4**, 957 (2004).
11. E. X. Jin and X. Xu, Appl. Phys. B **84**, 3 (2006).
12. K. D. Ko, A. Kumar, K. H. Fung, R. Ambekar, G. L. Liu, N. X. Fang, and K. C. Toussaint, Nano Lett. **11**, 61 (2011).
13. E. C. Kinzel and X. Xu, Opt. Lett. **35**, 992 (2010).
14. T. Sondergaard, S. I. Bozhevolnyi, J. Beermann, S. M. Novikov, E. Devaux, and T. W. Ebbesen, Nano Lett. **10**, 291 (2010).
15. N. C. Lindquist, P. Nagpal, A. Lesuffleur, D. J. Norris, and S. H. Oh, Nano Lett. **10**, 1369 (2010).
16. E. D. Palik, *Handbook of Optical Constants of Solids*, 3rd ed. (Academic, 1998).
17. COMSOL Multiphysics User's Guide, Version 3.4, COMSOL AB, Burlington, Mass. (2008).
18. D. Wei, R. Bachelot, S. Kostcheev, P. Royer, and R. Espiau de Lamaestre, J. Appl. Phys. **108**, 124314 (2010).
19. T. Grosjean, M. Mivelle, F. I. Baida, G. W. Burr, and U. C. Fischer, Nano Lett. **11**, 1009 (2011).
20. R. Ameling and H. Giessen, Nano Lett. **10**, 4394 (2010).
21. P. Genevet, J.-P. Tetienne, E. Gatzogiannis, R. Blanchard, M. A. Kats, M. O. Scully, and F. Capasso, Nano Lett. **10**, 4880 (2010).
22. I. A. Ibrahim, M. Mivelle, T. Grosjean, J. T. Allegre, G. W. Burr, and F. I. Baida, Opt. Lett. **35**, 2448 (2010).